scientific reports

Check for updates

OPEN

Hydrogen generation of single alloy Pd/Pt quantum dots over Co_3O_4 nanoparticles via the hydrolysis of sodium borohydride at room temperature

Mostafa Farrag[1]✉ & Gomaa A. M. Ali[2]

To satisfy global energy demands and decrease the level of atmospheric greenhouse gases, alternative clean energy sources are required. Hydrogen is one of the most promising clean energy sources due to its high chemical energy density and near-zero greenhouse gas emissions. A single alloyed phase of Pd/Pt nanoclusters as quantum dots (QDs) was prepared and loaded over Co_3O_4 nanoparticles with a low loading percentage (1 wt.%) for hydrogen generation from the hydrolysis of $NaBH_4$ at room temperature. L-glutathione (SG) was used as a capping ligand. It was found that the single alloy catalyst $(Pd_{0.5}–Pt_{0.5})_n(SG)_m/Co_3O_4$ caused a significant enhancement in hydrogen generation in comparison to the monometallic clusters $(Pd_n(SG)_m$ and $Pt_n(SG)_m)$. Moreover, the Pd/Pt alloy showed a positive synergistic effect compared to the physical mixture of Pd and Pt clusters (1:1) over Co_3O_4. The QDs alloy and monometallic Pd and Pt clusters exhibited well-dispersed particle size in ~ 1 nm. The $(Pd_{0.5}–Pt_{0.5})_n(SG)_m/Co_3O_4$ catalyst offers a high hydrogen generation rate (HGR) of 8333 mL min^{-1} g^{-1} at room temperature. The synergistic effect of Pd and Pt atoms in the nanoclusters alloy is the key point beyond this high activity, plus the prepared clusters' unique atomic packing structure and electronic properties. The effect of the $NaBH_4$ concentration, catalyst amount, and reaction temperature (25–60 °C) were investigated, where HGR reaches 50 L min^{-1} g^{-1} at 60 °C under the same reaction conditions. The prepared catalysts were analyzed by UV–Vis, TGA, HR-TEM, XRD, and N_2 adsorption/desorption techniques. The charge state of the Pd and Pt in monometallic and alloy nanoclusters is zero, as confirmed by X-ray photoelectron spectroscopy analysis. The catalysts showed high recyclability efficiency for at least five cycles due to the high leaching resistance of the alloy nanoclusters within the Co_3O_4 host. The prepared catalysts are highly efficient for energy-based applications.

Bimetallic systems as heterogeneous catalysts have received tremendous scientific and industrial attention due to their excellent catalytic performance compared to monometallic systems[1–3]. The synergistic effect and cooperative interactions between the two metals are the main reason beyond their activity, where the electrons transfer or exchange between the two metals in the bimetallic lattice enhances the catalytic activity of the bimetallic systems[1,2,4].

Recently, hydrogen as clean energy has been considered a key factor in the increasing depletion of fossil fuels and exacerbating the environmental pollution crisis[5,6]. Hydrogen is universally accepted as a clean energy source due to its relatively high energy density (142 MJ kg^{-1}) in comparison to diesel and gasoline (46 MJ kg^{-1}) and can reduce the amount of greenhouse gas and acid rain when used as fuel[7]. Hydrolysis of sodium borohydride ($NaBH_4$) has been reported to be a promising way to generate hydrogen due to its high hydrogen content (10.65 wt.%), low price, and nontoxicity ($NaBH_4 + 2H_2O \rightarrow NaBO_2 + 4H_2$, $\Delta H = -300$ kJ mol^{-1})[6–12]. Metal alloys such as NiB and CoB showed good activity in the hydrolysis of $NaBH_4$[9,10,13], where 5 wt. % CoB/CeO_2 showed

[1]Nanoclusters and Photocatalysis Laboratory, Chemistry Department, Faculty of Science, Assiut University, Assiut 71516, Egypt. [2]Chemistry Department, Faculty of Science, Al-Azhar University, Assiut 71524, Egypt. ✉email: mostafafarrag@aun.edu.eg

hydrogen generation rate (HGR) of 533 mL g^{-1} min^{-1}[10]. Patel et al.[14] reported the effect of electron transfer between metallic Co and B.

Noble metals such as Au, Pd, Ru, and Pt-based catalysts were reported as ideal candidates for hydrogen generation due to their excellent catalytic activity and high stability[11,12,15]. 20 wt.% of Ru (19.9 nm), Pd (12.2 nm), and Pt (3.2 nm) over Co_3O_4 showed high catalytic activity in hydrolysis of $NaBH_4$ with HGR of 6514, 4713, and 2109 mL g^{-1} min^{-1}, respectively[11]. Pt/Al_2O_3, Rh/Al_2O_3, and Pd/Al_2O_3 exhibited some catalytic activity in hydrolysis of 15–23 wt.% $NaBH_4$ solutions[16]. The bimetallic catalysts showed higher performance in the hydrolysis of $NaBH_4$ than the corresponding monometallic[17–23]. Pt-Ru bimetallic system over $LiCoO_2$ support exhibited catalytic activity in the hydrolysis of $NaBH_4$ more than the monometallic Ru or Pt[20]. The Ru-Co alloys over γ-Al_2O_3 showed higher HGR in $NaBH_4$ hydrolysis than single monometallic samples[21]. Ni – Pt/CeO_2 over granular activated carbon catalyst achieved complete and rapid decomposition of hydrazine hydrate to generate H_2 with a 100% selectivity at moderate temperature in the presence of 1 M NaOH[22]. Moreover, the salisylaldimine-Ni complex has shown 190% increment in $NaBH_4$ hydrolysis than pure Ni catalyst with a maximum hydrogen production rate of 2240 ml min^{-1} g^{-1}[24].

To prepare size-selected metal nanoclusters (quantum dots, QDs), a great deal of work should be done; for example, deposition of Pt clusters over single-crystal supports such as MoO_3 and TiO_2 under ultrahigh vacuum (UHV) conditions 10^{-9} mbar[25]. This model of catalysis is very complicated and largely deviated from the real world of catalytic conditions. Monolayer-protected nanoclusters of noble metals have recently gained much attention in the catalysis field due to their unique atomic packing structure and electronic properties[26–38]. In our previous work, platinum nanoclusters protected with l-cysteine and N-acetyl-l-cysteine over TiO_2 showed high catalytic activity in the oxidation of styrene[26] and solar degradation of methylene blue[38], respectively. Pd nanoclusters protected with N-acetyl-l-cysteine exhibited superior catalytic activity in hydrogenation of α, β-unsaturated aldehydes such as cinnamaldehyde[33]. Moreover, size-selected gold clusters ($Au_{25}(SCH_2CH_2Ph)_{18}$, $Au_{38}(SCH_2CH_2Ph)_{24,}$ and $Au_{144}(SCH_2CH_2Ph)_{60}$) over ceria showed high catalytic activity in the oxidation of carbon monoxide at a low temperature[35–37].

To the best of our knowledge, this is the first time to prepare a single alloyed Pd/Pt quantum dots (QDs) in regime of 1 nm by simple way in a large yield. A very low loading percentage (1 wt.%) from the prepared alloy over Co_3O_4 achieved a high hydrogen yield with a hydrogen generation rate (HGR) 8333 mL g^{-1} min^{-1}. Additionally, a comparison between the activity of the single alloy and the physical mixing of Pd and Pt nanoclusters was studied, where the alloy exhibited a positive synergistic effect and the physical mixing showed a negative synergistic effect. Where, the physical mixture of palladium and platinum nanoclusters (1:1) was loaded over the Co_3O_4 nanoparticles for comparison. 1 wt.% $(Pd_{0.5}–Pt_{0.5})_n(SG)_m/Co_3O_4$ catalyst showed the best catalytic activity in $NaBH_4$ hydrolysis reaction to generate hydrogen gas. However, the physical mixing of Pd and Pt nanoclusters over Co_3O_4 showed lower activity than monometallic platinum clusters. The synergistic effect between Pd and Pt atoms in the nanoclusters alloy plays the main role in this activity. As confirmed by HR-TEM, the particle size of palladium, platinum, and single alloy nanoclusters is around 1 nm. The stoichiometric ratio between the metallic and organic parts in the three prepared nanoclusters was determined by TG analysis. The crystallinity and surface area of the loaded nanoclusters over Co_3O_4 were measured by X-ray diffraction (XRD) and N_2 adsorption/desorption isotherms at – 196 °C. X-ray photoelectron spectroscopy (XPS) confirmed that the charge of Pd and Pt in the monometallic and bimetallic nanoclusters is zero.

Experimental

Chemicals. Potassium hexachloropalladate (IV) (K_2PdCl_6, 98%, Sigma–Aldrich), chloroplatinic acid ($H_2PtCl_6.6H_2O$, ≥ 37.5% Pt basis, Sigma–Aldrich), sodium borohydride ($NaBH_4$, ≥ 96%, Aldrich), l-glutathione (99%, Sigma–Aldrich) and ethanol were used for preparing the protected Pd and Pt nanoclusters and the Pd–Pt alloy nanoclusters. Cobalt (II, III) oxide (Co_3O_4) nanopowder, < 50 nm particle size (99.5%, Sigma–Aldrich), was used as active support. All chemicals were used as received. All glassware was thoroughly cleaned with aqua regia ($HCl:HNO_3$ = 3:1 v/v), rinsed with double distilled water and ethanol, and dried in an oven before use.

Preparation of $Pd_n(SG)_m$ nanoclusters. 79.466 mg potassium hexachloropalladate (IV) (K_2PdCl_6, 0.2 mmol) was dissolved in 10 mL double-distilled water, 43.02 mg l-glutathione (0.14 mmol) was dissolved in 3 mL double-distilled water, and added to the palladium solution, under vigorously stirring (~ 1100 rpm) at room temperature. During the addition of the l-glutathione solution, the orange color of the palladium salt solution became light orange, and then the color changed to red. After 30 min. of stirring, a freshly prepared aqueous solution of $NaBH_4$ (75.66 mg, 2 mmol, dissolved in 3 mL double-distilled water) was added dropwise over the resulting solution while stirring vigorously (~ 1100 rpm). The red solution converted quickly to black, indicating the reduction of the palladium salt and the formation of palladium nanoclusters. The reaction was allowed to proceed under constant stirring for 1 h. The mixture was evaporated under a vacuum to near dryness, and then the particles were precipitated by adding ethanol. The black-brown precipitate was re-dissolved in double-distilled water and re-precipitated by ethanol. This step should be repeated three times to remove excess $NaBH_4$. The resulting precipitate was then collected through centrifugal precipitation and washed with ethanol to remove the unreacted material. The black-brown solid consisting of $Pd_n(SG)_m$ nanoclusters was finally dried overnight at 100 °C[26–38].

Preparation of $Pt_n(SG)_m$ nanoclusters. 81.96 mg chloroplatinic acid ($H_2PtCl_6.6H_2O$, 0.2 mmol) was dissolved in 10 mL double-distilled water, and 43.02 mg l-glutathione (0.14 mmol) was dissolved in 3 mL double distilled water and added to the platinum solution, under vigorously stirring (~ 1100 rpm) at room temperature. During the addition of the l-glutathione solution, the yellow solution of platinum salt showed some turbidity

after adding the ligand, then the color changed to orange and finally to canary yellow. After 30 min stirring, a freshly prepared aqueous solution of $NaBH_4$ (75.66 mg, 2 mmol, dissolved in 3 mL double-distilled water) was added dropwise over the resulting solution while stirring vigorously (~1100 rpm). The canaries yellow color solution converted gradually to black, indicating the reduction of the platinum salt and formation of platinum nanoclusters. The reaction was allowed to proceed under constant stirring for 1 h. Then, the $Pt_n(SG)_m$ nanoclusters were separated, purified, and dried as described in the case of $Pd_n(SG)_m$ nanoclusters[26].

Preparation of $(Pd_{0.5}–Pt_{0.5})_n(SG)_m$ nanoclusters. 40.98 mg chloroplatinic acid ($H_2PtCl_6.6H_2O$, 0.1 mmol) was dissolved in 5 mL double-distilled water (solution A). 32.73 mg potassium tetrachloropalladate (II) (K_2PdCl_4, 0.1 mmol) was dissolved in 5 mL double-distilled water (solution B). Solution A was mixed with solution B for 30 min., and then 43.02 mg l-glutathione (0.14 mmol) was dissolved in 3 mL double-distilled water and added to the solution vigorously stirring (~1100 rpm) at room temperature. The l-glutathione solution reacted with the mixed solutions of the two salts simultaneously. After adding the ligand, the yellow solution showed some turbidity; then the color changed to orange and finally to canary yellow. After 30 min. stirring, a freshly prepared aqueous solution of $NaBH_4$ (75.66 mg, 2 mmol, dissolved in 3 mL double-distilled water) was added dropwise over the resulting solution while stirring vigorously (~1100 rpm). The canaries yellow color solution converted gradually to black, indicating the platinum and palladium salts reduced simultaneously to form Pd–Pt single alloy nanoclusters. The reaction was allowed to proceed under constant stirring for 1 h. Then, the $(Pd_{0.5}–Pt_{0.5})_n(SG)_m$ alloy was separated, purified, and dried as described in the case of $Pd_n(SG)_m$ nanoclusters[26,38].

Loading of the prepared nanoclusters over Co_3O_4. The 1 wt.% of catalysts ($Pd_n(SG)_m/Co_3O_4$, $Pt_n(SG)_m/Co_3O_4$, $Pd_n(SG)_m + Pt_n(SG)_m/Co_3O_4$ and $(Pd_{0.5}–Pt_{0.5})_n(SG)_m/Co_3O_4$) were prepared by a well-known impregnation method. 0.5 g of Co_3O_4 nanoparticles were suspended in 50 mL double-distilled water in an ultrasonic bath for 30 min., 5 mg of the clusters were dissolved in 10 mL double-distilled water, and then added to the Co_3O_4 slurry. The slurry was stirred 24 h at room temperature, and then the loaded catalyst was collected by centrifuge at 6000 rpm, for 10 min. The brown color of the clusters solution becomes colorless, confirming the transfer of all clusters amount to the Co_3O_4 surface. The loaded catalysts were dried in an oven at 100 °C overnight[26,38].

The catalytic reaction for the hydrolysis of $NaBH_4$. The hydrolysis of $NaBH_4$ has been performed at room temperature (25 °C), over 5 mg of the prepared catalysts ($Pd_n(SG)_m/Co_3O_4$, $Pt_n(SG)_m/Co_3O_4$, $Pd_n(SG)_m + Pt_n(SG)_m/Co_3O_4$, and $(Pd_{0.5}–Pt_{0.5})_n(SG)_m/Co_3O_4$). 1 g of $NaBH_4$ was added to 100 mL of water (corresponding to 1 wt.%), and the catalyst was added. The reaction solution was stirred at 1000 rpm. The hydrogen-generated volume was measured using the water displacement method[9–12]. $(Pd_{0.5}–Pt_{0.5})_n(SG)_m/Co_3O_4$ was used as a model catalyst to study the effect of catalyst weight (5, 15, 30, and 50 mg) in the hydrolysis of 1 wt.% $NaBH_4$ solution at 25 °C.

5 mg of the $(Pd_{0.5}–Pt_{0.5})_n(SG)_m/Co_3O_4$ catalyst was chosen to employ different $NaBH_4$ solutions such as 0.189, 0.5, 1, and 2 wt.%. The same amount of the catalyst was used to follow up the reaction at different temperatures 25, 45, and 60 °C, of the 1 wt.% $NaBH_4$ solution.

In the recyclability study, 5 mg of $(Pd_{0.5}–Pt_{0.5})_n(SG)_m/Co_3O_4$ catalyst was repeatedly used five times to generate H_2 using 1 wt.% $NaBH_4$ solution at 25 °C. Once the hydrolysis reaction of $NaBH_4$ was completed, a new $NaBH_4$ solution was added for a second cycle, and so on.

Results and discussion

Optical properties and chemical composition of the prepared nanoclusters. Metal nanoclusters exhibit some absorption in a visible region, and these absorptions come from the excitation of plasmon resonance electrons or interband transitions[26,30,31,33,38]. These absorption peaks' positions and width depend on the metal type, particle size, protecting ligand, and chemical charge[26,29,31,33,38]. Pt nanoparticles in regime 4–10 nm show an absorption peak at 215 nm[39,40]. The intensity of this peak decreases by decreasing particle size and is essentially undetectable for smaller clusters less than 2 nm[41]. S-containing Pd(II) complexes exhibited surface plasmon peak at 350–500 nm, corresponding to the charge transfer between the metal and ligand[42].

The prepared Pd and Pt nanoclusters and Pd/Pt alloy nanoclusters in water show featureless absorption curves in the UV–vis region, where their color is dark brown (Fig. 1-I). These absorption curves agree with the theoretical calculations by Creighton and Eadon[39]. As shown in Fig. 1-I, there are no peaks or noise in the 350–500 nm region, indicating the prepared nanoclusters are pure from the intermediated complex (Pd(II)-SG), and all the palladium ions are reduced to Pd(0)[33]. Moreover, the prepared nanoclusters are pure from the unreacted l-glutathione ligand, which shows one absorption peak at 224 nm[38].

Thermogravimetric analysis (TGA) is used to obtain the ratio between the organic and metallic parts in the protected nanoclusters[26,29,31,33,38]. Therefore, the metal-to-ligand ratio (M/L) and the average chemical formula of the MPCs can be estimated. Figure 1-II shows the TGA curves of the prepared nanoclusters and the pure ligand. According to the TGA curves, the protecting ligand in $Pd_n(SG)_m$, $Pt_n(SG)_m$, and $(Pd_{0.5}–Pt_{0.5})_n(SG)_m$ nanoclusters decompose in two decomposition steps. The ligand decomposition is completed at 900 °C; the residual is the metallic part. The weight percentage of the metallic part of the prepared nanoclusters $Pd_n(SG)_m$, $Pt_n(SG)_m$, and $(Pd_{0.5}–Pt_{0.5})_n(SG)_m$ are 50.18, 62.1, and 56 wt. % (Table 1). The average metal/ligand ratio (M/L) and the average molecular formula of the prepared nanoclusters are calculated and summarized in Table 1[26,38].

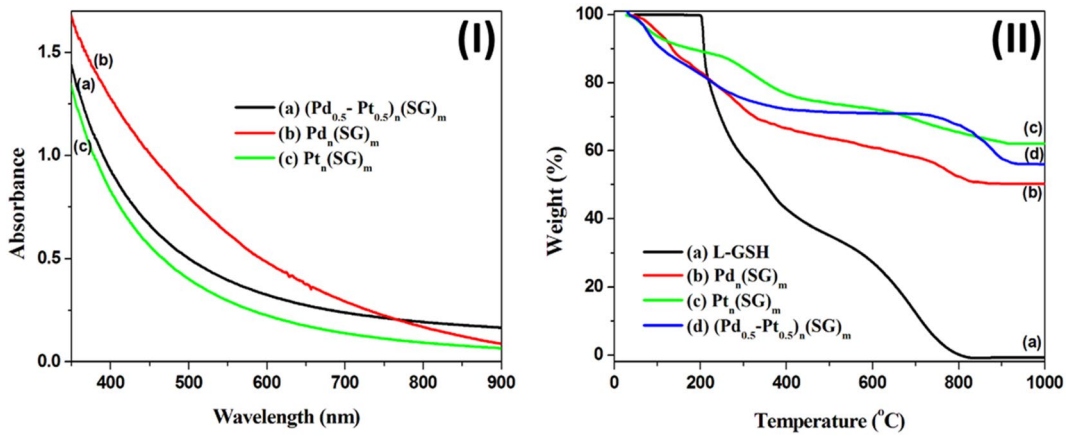

Figure 1. (**I**) UV–Vis absorption spectra of the prepared nanoclusters $(Pd_{0.5}–Pt_{0.5})_n(SG)_m$ (a), $Pd_n(SG)_m$ (b), and $Pt_n(SG)_m$ (c). The prepared clusters show featureless absorption curves in the visible region of 350–900 nm. (**II**) The thermogravimetric analysis (TGA) of the prepared clusters ($(Pd_{0.5}–Pt_{0.5})_n(SG)_m$ (a), $Pd_n(SG)_m$ (b), and $Pt_n(SG)_m$ (c)) and the protecting ligand l-glutathione (d).

Catalysts	Weight (%) at 900 °C	M/S ratio	Molecular formula
$(Pd_{0.5}–Pt_{0.5})_n(SG)_m$	56.00	1:0.38	$(Pd–Pt)_{3n}L_n$
$Pd_n(SG)_m$	50.18	1:0.34	$Pd_{3n}L_n$
$Pt_n(SG)_m$	62.10	1:0.30	$Pt_{3n}L_n$

Table 1. The thermogravimetric analysis data for the prepared nanoclusters.

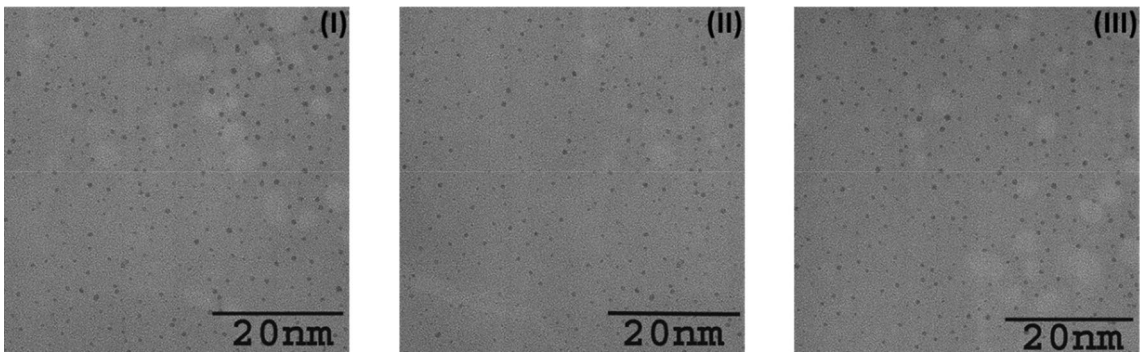

Figure 2. High resolution-transmission electron microscopy (HR-TEM) images of the prepared clusters $Pd_n(SG)_m$ (**I**), $Pt_n(SG)_m$ (**II**), and $(Pd_{0.5}–Pt_{0.5})_n(SG)_m$ (**III**). The three clusters show a monodisperse particle size of around 1 nm.

The particles size and charge of the prepared nanoclusters. High resolution-transmission electron microscopy (HR-TEM) was used to measure the particle size of the prepared nanoclusters. Figure 2 (I, II, and III) shows the HR-TEM images of the $Pd_n(SG)_m$, $Pt_n(SG)_m$, and $(Pd_{0.5}–Pt_{0.5})_n(SG)_m$, respectively. The particle size of the prepared clusters is ~ 1 nm, which appears as QDs. The single alloy QDs $(Pd_{0.5}–Pt_{0.5})_n(SG)_m$ shows a particle size that is uniformly distributed similar to the monometallic nanoclusters $(Pd_n(SG)_m$ and $Pt_n(SG)_m)$. This indicates that the method can be used for bimetallic and monometallic QDs preparation.

The particle charge of the prepared nanoclusters is characterized by X-ray photoelectron spectroscopy (XPS). The Pd 3d XPS spectrum of the $Pd_n(SG)_m$ clusters is shown in Fig. 3-I. The binding energies of the Pd $3d^{5/2}$ and $3d^{3/2}$ electrons are at 335.42 and 340.66 eV[16] respectively, corresponding to Pd(0). These findings are in agreement with those obtained for Pd nanoparticles loaded on Co_3O_4 nanoparticles[43,44]. Figure 3-II shows the XPS spectrum of platinum atoms in $Pt_n(SG)_m$ clusters, the binding energies of the Pt $4F^{5/2}$ and $4F^{7/2}$ electrons are 74.58 and 71.19 eV, respectively, that are corresponding to Pt(0)[45]. The charge of Pd and Pt atoms in the single alloy nanoclusters $(Pd_{0.5}–Pt_{0.5})_n(SG)_m$ are also zero, as confirmed by XPS analysis (Fig. 3-III,IV), where the binding energies of the Pd $3d^{5/2}$ and $3d^{3/2}$ electrons are 335.44 and 340.70 eV, and for Pt $4F^{5/2}$ and $4F^{7/2}$ electrons are 74.36 and 71.02 eV, respectively. The absence of the two peaks of Pd^{4+} at 339.2 and 342.9 eV indicates the presence of Pd in metallic form (neither as PdO_2 nor $Pd(OH)_4$)[43].

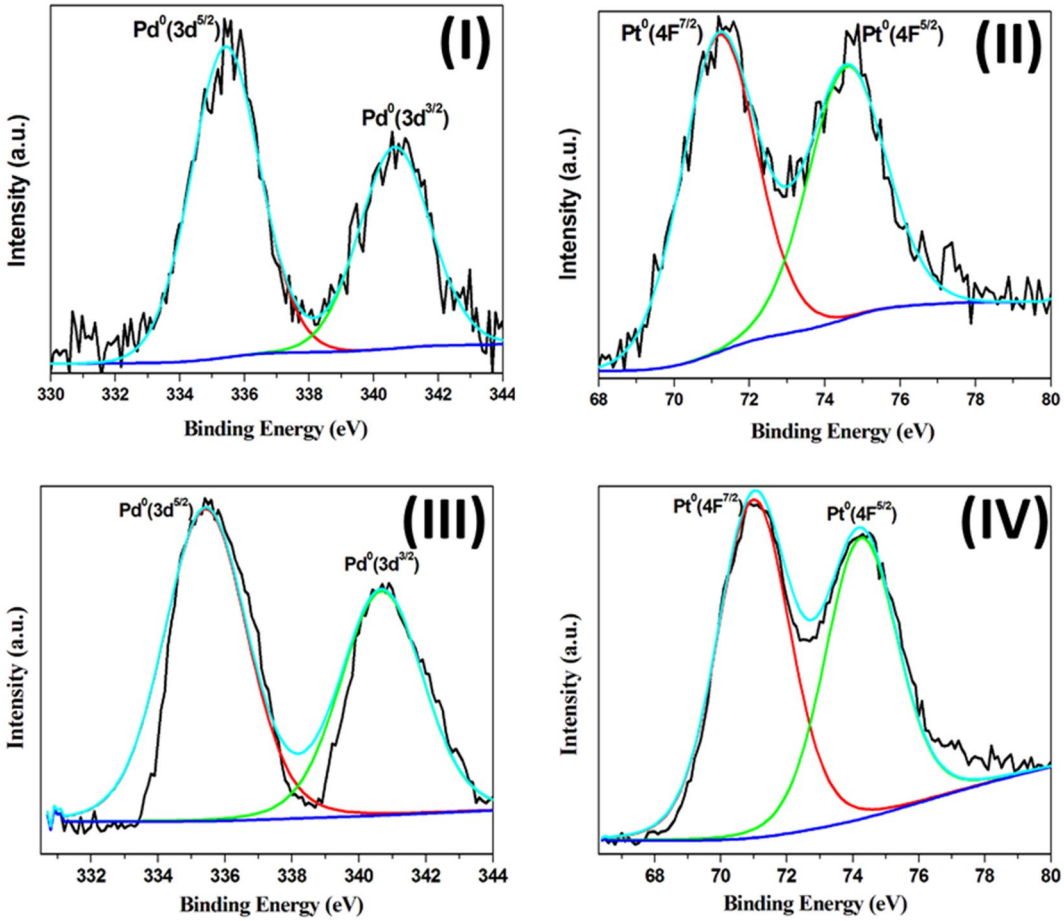

Figure 3. High resolution-XPS spectra of (**I**) Pd $3d^{5/2}$ and $3d^{3/2}$ electrons in $Pd_n(SG)_m$ clusters, (**II**) Pt $4F^{5/2}$ and $4F^{7/2}$ electrons in $Pt_n(SG)_m$ clusters, (**III**) Pd atoms in the single alloy nanoclusters ($(Pd_{0.5}–Pt_{0.5})_n(SG)_m$), and (**IV**) Pt atoms in the single alloy nanoclusters ($(Pd_{0.5}–Pt_{0.5})_n(SG)_m$).

Texture properties and crystallinity of the prepared catalysts. Liquid nitrogen at − 196 °C is used to determine the surface texture properties of the pure support (Co_3O_4) and the doped Co_3O_4 with the prepared nanoclusters ($Pd_n(SG)_m/Co_3O_4$, $Pt_n(SG)_m/Co_3O_4$, $Pd_n(SG)_m + Pt_n(SG)_m/Co_3O_4$ and $(Pd_{0.5}–Pt_{0.5})_n(SG)_m/Co_3O_4$) by measuring the adsorption/desorption isotherms (Fig. 4). According to the IUPAC classification of hysteresis loops, the sorption isotherms of the prepared catalysts and the pure support are type H3 hysteresis loops[46–48]. The surface areas of the prepared catalysts and support are summarized in Table 2. The values of surface area that are measured by BET equation (S_{BET}) and T-method (S_t) for all the investigated catalysts are close to each other, which confirms the correct choice of standard t-curves for pore analysis and indicates the absence of ultra-micropores in these catalysts[26,33].

X-ray diffraction is used to measure the crystallinity of the prepared catalysts. Figure 5 illustrates the XRD diffractograms of the prepared catalysts and Co_3O_4. The characteristic diffraction planes of the Co_3O_4 are (111), (220), (311), (222), (400), (422), (511) and (440) appear at 2θ equal to 19.0°, 31.2°, 36.7°, 38.5°, 44.8°, 55.5°, 59.3° and 65.4°, respectively (Fig. 5a)[49,50]. The prepared catalysts show the same XRD pattern as pure Co_3O_4, and no new peaks related to the presence of Pd or Pt clusters are detected, where the doping percentage is very low (1 wt.%) (Fig. 5b–e). This means the crystallinity of pure Co_3O_4 does not affect loading with the prepared clusters. Also, there is no significant difference in either diffraction angle or peak width between the Co_3O_4 and prepared catalysts, indicating that the crystal structure of Co_3O_4 is not affected by doping. The crystalline size (d_{Co3O4}) of bare Co_3O_4 is calculated using Debye–Scherrer Equations[51] as 20 nm for the broadening of (311) peak reflection (Fig. 5). The d_{Co3O4} value for 1 wt.% $(Pd_{0.5}–Pt_{0.5})_n(SG)_m/Co_3O_4$ catalyst is less than bare Co_3O_4 18.6 nm (Fig. 5)[26,33].

The catalytic activity of the prepared catalysts. The hydrolysis reaction of $NaBH_4$ for hydrogen generation is chosen as a model reaction to estimate the catalytic activities of Pd_n, Pt_n, physical mixture ($Pd_n + Pt_n$) clusters and the single alloy clusters $(Pd_{0.5}–Pt_{0.5})_n$ over Co_3O_4 nanoparticles as support. Figure 6 shows the volume of generated hydrogen at room temperature (25 °C) against reaction time over the prepared catalysts. 5 mg of 1 wt.% $Pd_n(SG)_m/Co_3O_4$ catalyst produces the maximum hydrogen volume i.e. 500 mL from the hydrolysis of $NaBH_4$ solution (1 g $NaBH_4$ in 100 mL H_2O) within 26 min. stirring. $Pt_n(SG)_m$ nanoclusters over Co_3O_4 show more activity than Pd clusters in the hydrolysis of $NaBH_4$ solution, where the $Pt_n(SG)_m/Co_3O_4$ catalyst produces

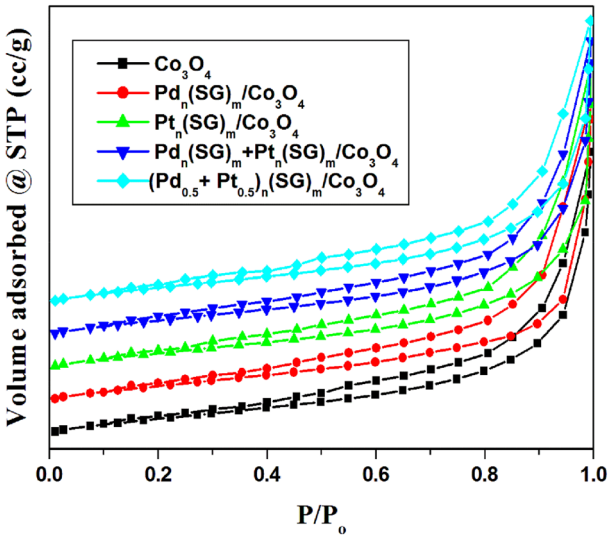

Figure 4. N_2 adsorption/desorption isotherms of the prepared catalysts and pure support show sorption isotherms type H3 according to the IUPAC classification.

Catalysts	S_{BET} ($m^2\ g^{-1}$)	S_t ($m^2\ g^{-1}$)
$(Pd_{0.5}–Pt_{0.5})_n(SG)_m/Co_3O_4$	56.3	56.3
$Pd_n(SG)_m + Pt_n(SG)_m/Co_3O_4$	54.7	54.7
$Pd_n(SG)_m/Co_3O_4$	56.8	56.8
$Pt_n(SG)_m/Co_3O_4$	55.2	55.2
Co_3O_4	60.3	60.3

Table 2. Specific surface area data for the prepared catalysts and pure support.

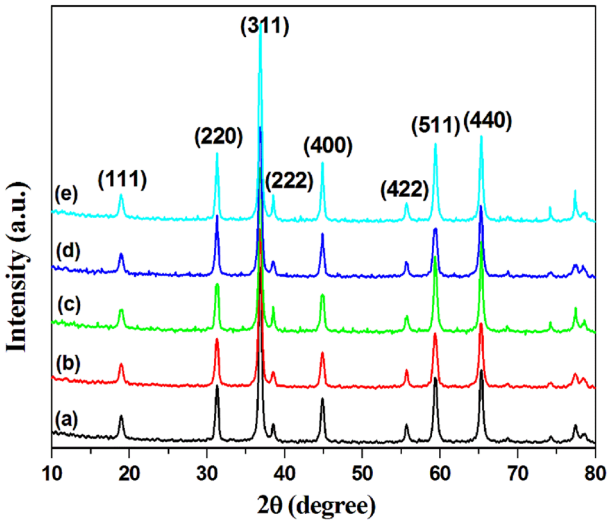

Figure 5. X-ray diffractograms of the pure Co_3O_4 support (a), and prepared catalysts: $Pd_n(SG)_m/Co_3O_4$ (b), $Pt_n(SG)_m/Co_3O_4$ (c), $Pd_n(SG)_m + Pt_n(SG)_m/Co_3O_4$ (d), and $Pd_{0.5}–Pt_{0.5})_n(SG)_m/Co_3O_4$ (e).

the maximum hydrogen volume within 18 min. stirring at room temperature (Fig. 6). However, the physical mixing of Pd and Pt clusters over Co_3O_4 with the same doping percentage (~ 1 wt.%) shows lower catalytic activity than 1 wt. % $Pt_n(SG)_m/Co_3O_4$ catalyst. Surprisingly, the single alloy of Pd and Pt QDs ($Pd_{0.5}–Pt_{0.5})_n(SG)_m/Co_3O_4$) shows amazing catalytic activity, where it reaches the maximum hydrogen volume i.e. 500 mL, within

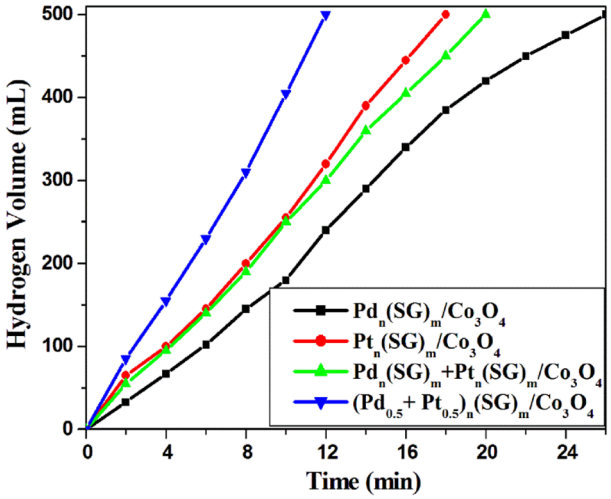

Figure 6. Hydrogen generation from $NaBH_4$ hydrolysis over the prepared catalysts. Reaction conditions: 1 g of $NaBH_4$ in 100 H_2O; catalyst, 5 mg; at 25 °C.

Catalysts	HGR (mL min^{-1} g^{-1})
$(Pd_{0.5}–Pt_{0.5})_n(SG)_m/Co_3O_4$	8333
$Pd_n(SG)_m + Pt_n(SG)_m/Co_3O_4$	5000
$Pt_n(SG)_m/Co_3O_4$	5555
$Pd_n(SG)_m/Co_3O_4$	3846

Table 3. Hydrogen generation rate (HGR) for $NaBH_4$ hydrolysis reaction over different catalysts. Catalytic test: 1 g of $NaBH_4$ in 100 H_2O; Catalyst, 5 mg; at 25 °C.

only 12 min. stirring (Fig. 6) with HGR of 8333 mL min^{-1} g^{-1}. The HGRs for the $NaBH_4$ hydrolysis reaction over the prepared catalysts are summarized in Table 3.

The excellent synergetic interaction between Pd and Pt atoms in the single alloy $(Pd_{0.5}–Pt_{0.5})_n(SG)_m$ QDs plays a crucial role in the observed high catalytic activity. This positive synergistic effect does not appear in the physical mixing of nanoclusters over the support $(Pd_n(SG)_m + Pt_n(SG)_m/Co_3O_4)$ by the same doping percentage. Since there are two types of synergetic effect (positive and negative)[52], if the qualitative effect of electronic interaction between the components of the bimetallic system and the geometric effects due to changes in lattice constants are in the same direction as the bimetallic system will enhance the reaction effectively in comparison to the monometallic systems. However, if the electronic and geometric effect direction is opposite, the lower activity will be received[52].

Figure 7 shows the effect of catalyst weight on the hydrolysis of $NaBH_4$. $(Pd_{0.5}–Pt_{0.5})_n(SG)_m/Co_3O_4$ catalyst was chosen to study this factor. 5, 15, 30, and 50 mg of the catalyst were added to the $NaBH_4$ solution (1 g $NaBH_4$ in 100 mL H_2O) at room temperature (25 °C). As shown in Fig. 7, the time to reach the maximum hydrogen volume (500 mL) decreases with the increase in the weight of the catalyst. Where the time to reach the maximum hydrogen volume decreases from 12.0 to 1.5 min. over 5 and 50 mg of $(Pd_{0.5}–Pt_{0.5})_n(SG)_m/Co_3O_4$, respectively (Fig. 7).

Different concentrations of $NaBH_4$ solution (0.189, 0.5, 1 and 2 wt.%) were tested over 5 mg of $(Pd_{0.5}–Pt_{0.5})_n(SG)_m/Co_3O_4$ catalyst at 25 °C (Fig. 8-I). The reaction time decreases with the increase of the $NaBH_4$ concentration. The maximum hydrogen volume was reached within 19, 15, 12, and 9 min. of the 0.189, 0.5, 1, and 2 wt.% $NaBH_4$ solution over $(Pd_{0.5}–Pt_{0.5})_n(SG)_m/Co_3O_4$ catalyst, respectively (Fig. 8-I). The effect of reaction temperature was also tested for hydrogen generation from the 1 wt.% $NaBH_4$ solution over 5 mg of $(Pd_{0.5}–Pt_{0.5})_n(SG)_m/Co_3O_4$ catalyst (Fig. 8-II). The reaction was measured at different temperatures at 25, 45, and 60 °C; the reaction time decreased with the temperature increasing (Fig. 8-II). The maximum hydrogen volume was reached within only 2 min stirring over 5 mg of $(Pd_{0.5}–Pt_{0.5})_n(SG)_m/Co_3O_4$ catalyst at 60 °C with HGR 50,000 mL min^{-1} g^{-1} (Fig. 8-II).

The best property of heterogeneous catalysis is easily separating the catalyst from the reaction mixture and reusing it until its activity decreases[26–28,32,33,38]. Thus, the ability of the $(Pd_{0.5}–Pt_{0.5})_n(SG)_m/Co_3O_4$ catalyst to recycle is tested for the hydrolysis of 1 wt. % $NaBH_4$ solution at room temperature using 5 mg from the catalyst. After each run, the catalyst was collected and reused without any treatment. The HGRs values were nearly identical for the 5 cycles (Fig. 9). These results reveal that the $(Pd_{0.5}–Pt_{0.5})_n(SG)_m/Co_3O_4$ catalyst can be reused, and their catalytic activity is quite consistent without significant change.

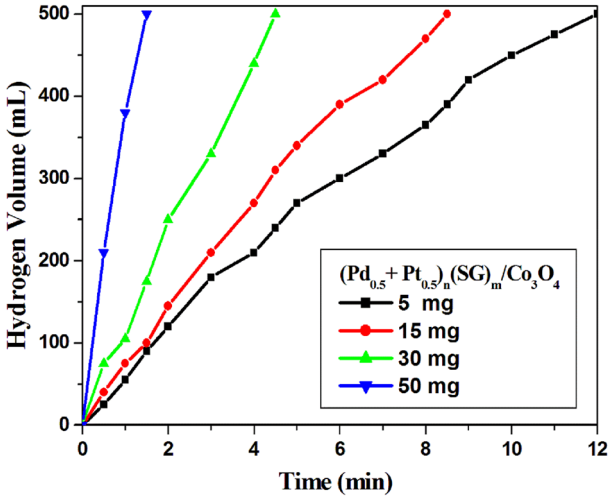

Figure 7. Effect of catalyst weight for hydrogen generation from the hydrolysis of $NaBH_4$ over 1 wt.% $(Pd_{0.5}–Pt_{0.5})_n(SG)_m/Co_3O_4$. Reaction conditions: 1 g of $NaBH_4$ in 100 H_2O; catalyst, 5–50 mg; at 25 °C.

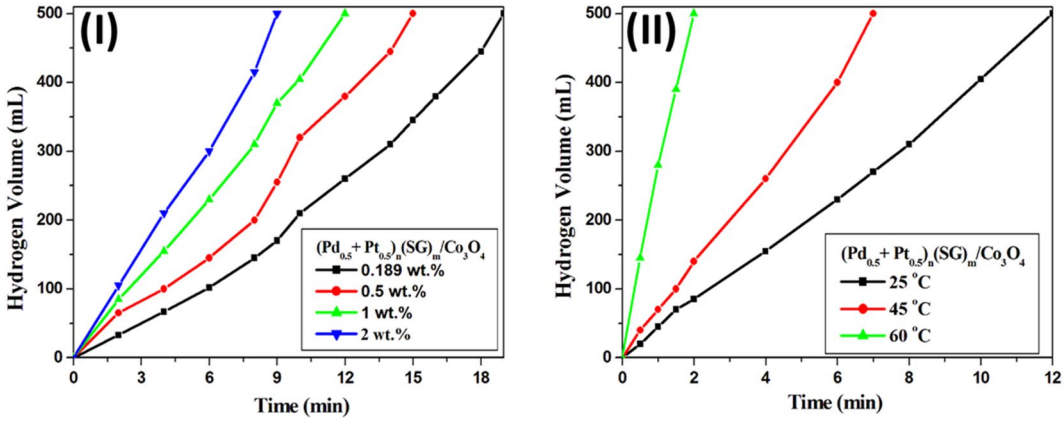

Figure 8. (**I**) Effect of $NaBH_4$ amount for hydrogen generation over 1 wt.% $(Pd_{0.5}–Pt_{0.5})_n(SG)_m/Co_3O_4$. Reaction conditions: 0.189, 0.5, 1 and 2 g $NaBH_4$ amount in 100 H_2O; Catalyst, 5 mg; at 25 °C. (**II**) Effect of reaction temperature for hydrogen generation from the hydrolysis of $NaBH_4$ over 1 wt.% $(Pd_{0.5}–Pt_{0.5})_n(SG)_m/Co_3O_4$. Reaction conditions: 1 g of $NaBH_4$ in 100 H_2O; catalyst, 5 mg; at 25–60 °C.

The $NaBH_4$ hydrolysis reaction mechanism can be further illustrated in view of Langmuir–Hinshelwood model. Where, Kojima et al.[53] reported the hydrolysis mechanism of $NaBH_4$ over $Pt/LiCoO_2$ catalyst, according to the Langmuir–Hinshelwood model. It was found that BH_4^- ions are adsorbed on Pt, while H_2O molecules are adsorbed on the oxide support to give H_2 and $B(OH)_4^-$[53]. These findings were confirmed by Liu et al.[54] using X-ray absorption. Co_3O_4 played the same role as $LiCoO_2$ for Pt/Co_3O_4 catalyst as claimed by Hung et al.[55]. The suggested mechanism of $NaBH_4$ hydrolysis over the $(Pd_{0.5}–Pt_{0.5})_n(SG)_m/Co_3O_4$ catalyst is demonstrated in Fig. 10, according to the Langmuir–Hinshelwood model. The catalytic process involves two different adsorption sites. The first site is suggested to be electron-rich Pt^0 and Pd^0 nanoclusters, whereas the second site is electron-deficient ($Co^{\delta+}$). The hydrolysis of the four hydrides of BH_4^- occurs one after the other by reaction with one adsorbed H_2O for each hydride (Fig. 10)[56].

A comparison with different catalysts used for hydrogen generation via $NaBH_4$ hydrolysis is listed in Table 4. As shown in Table 4, the prepared catalysts in this work showed superior catalytic activity in hydrogen generation from the hydrolysis of $NaBH_4$ using a relatively low noble metal loading (1 wt.%). Where $(Pd_{0.5}–Pt_{0.5})_n(SG)_m/Co_3O_4$ catalyst showed the highest hydrogen yield in the Table 4 with HGR equal to 8333 mL g^{-1} min^{-1}. Moreover, 1 wt.% loading percentage of monometallic Pt and Pd clusters over Co_3O_4 exhibited HGR 5555 and 3846 mL g^{-1} min^{-1}, however, the 20 wt.% Pt and Pd nanoparticles over the same support exhibited only 4713 and 2109 mL g^{-1} min^{-1}[11]. This high catalytic activity is due to the unique atomic packing structure and electronic properties of the nanoclusters.

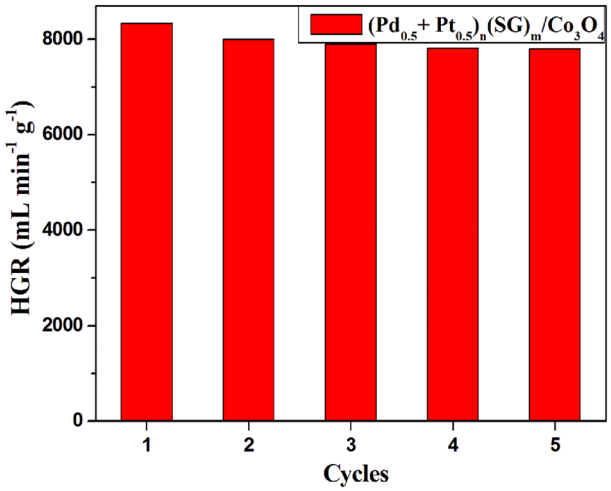

Figure 9. Recyclability of 1 wt.% $(Pd_{0.5}–Pt_{0.5})_n(SG)_m/Co_3O_4$ catalyst for hydrogen generation from the hydrolysis of $NaBH_4$. Reaction conditions: 1 g of $NaBH_4$ in 100 H_2O; catalyst, 5 mg; at 25 °C.

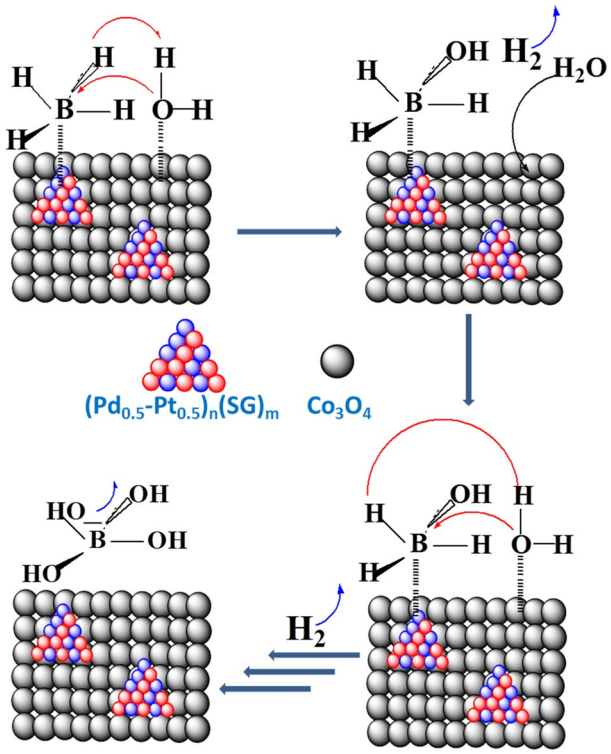

Figure 10. Suggested mechanism of $NaBH_4$ hydrolysis over $(Pd_{0.5}–Pt_{0.5})_n(SG)_m/Co_3O_4$ catalyst, according to the Langmuir–Hinshelwood model.

Conclusions

In conclusion, a single alloy of Pd/Pt quantum dots over Co_3O_4 $(Pd_{0.5}–Pt_{0.5})_n(SG)_m/Co_3O_4$ exhibited promising catalytic activity in hydrogen generation from the hydrolysis of $NaBH_4$. The maximum hydrogen volume i.e. 500 mL was reached within only 12 min. of stirring at room temperature with HGR 8333 mL min^{-1} g^{-1}. However, the physical mixing of the prepared two clusters $(Pd_n(SG)_m$ and $Pt_n(SG)_m)$ over Co_3O_4 exhibited a lower hydrogen yield in comparison to the single alloy clusters. The time to reach the maximum hydrogen volume decreases with the increase of the $(Pd_{0.5}–Pt_{0.5})_n(SG)_m/Co_3O_4$ catalyst weight (5, 15, 30, and 50 mg). Moreover, the effect of $NaBH_4$ concentration (0.189, 0.5, 1 and 2 wt.%) over 5 mg of $(Pd_{0.5}–Pt_{0.5})_n(SG)_m/Co_3O_4$ catalyst at 25 °C was studied. The hydrolysis of the $NaBH_4$ reaction was measured at different temperatures of 25, 45, and 60 °C, where 5 mg of $(Pd_{0.5}–Pt_{0.5})_n(SG)_m/Co_3O_4$ catalyst produced the maximum hydrogen volume within only

Catalysts	Catalyst mass (mg)	$NaBH_4$ (wt.%)	HGR (mL min^{-1} g^{-1})	Ref
5.4 wt.% Ru/Al_2O_3	500	10	65.5	[57]
Pt–Pd/CNT	–	0.1	126	[58]
10 wt.% $PtRu/LiCoO_2$	125	5	30	[20]
2 wt.% Ru/MMT	32	1	541	[59]
5 wt.%CoB/CeO_2	200	1	533	[10]
3 wt.% Ru/graphite	300	10	666.6	[60]
20 wt.% Pd/Co_3O_4	50	10	2109	[11]
$Pt/LiCoO_2$	50	20	3100	[53]
20 wt.% Pt/Co_3O_4	50	10	4713	[11]
1 wt.%$(Pd_{0.5}–Pt_{0.5})_n(SG)_m/Co_3O_4$	5	1	8333	This Work
1 wt.% $Pt_n(SG)_m/Co_3O_4$			5555	
1 wt.% $Pd_n(SG)_m/Co_3O_4$			3846	

Table 4. Comparison among catalysts used for the hydrolysis of $NaBH_4$ for hydrogen generation.

2 min stirring at 60 °C, with HGR 50,000 mL min^{-1} g^{-1}. The extremely catalytic activity of this catalyst attributes to the ultra-small particle size and the synergistic effect between Pd and Pt atoms in the alloy quantum dots.

Data availability

All data generated or analyzed during this study are included in this published article (and its Supplementary Information files).

Received: 16 June 2022; Accepted: 22 September 2022
Published online: 11 October 2022

References

1. Rai, R. K. *et al.* Access to highly active Ni–Pd bimetallic nanoparticle catalysts for C–C coupling reactions. *Catal. Sci. Technol.* **6**, 5567–5579. https://doi.org/10.1039/c6cy00037a (2016).
2. Wang, D., Villa, A., Porta, F., Su, D. & Prati, L. Single-phase bimetallic system for the selective oxidation of glycerol to glycerate. *Chem. Commun.* https://doi.org/10.1039/b518069d (2006).
3. Şahin, Ö., Kılınç, D. & Saka, C. Bimetallic Co–Ni based complex catalyst for hydrogen production by catalytic hydrolysis of sodium borohydride with an alternative approach. *J. Energy Inst.* **89**, 617–626. https://doi.org/10.1016/j.joei.2015.05.007 (2016).
4. Farrag, M. Ultrasmall bimetallic Ru-Co alloy nanoclusters immobilized in amino-functionalized UiO-66 and N-doped carbonaceous zirconium oxide nanocomposite for hydrogen generation. *J. Alloy. Compd.* **920**, 165893. https://doi.org/10.1016/j.jallcom.2022.165893 (2022).
5. Şahin, Ö., Kılınç, D. & Saka, C. Hydrogen generation from hydrolysis of sodium borohydride with a novel palladium metal complex catalyst. *J. Energy Inst.* **89**, 182–189. https://doi.org/10.1016/j.joei.2015.02.005 (2016).
6. Kılınç, D., Saka, C. & Şahin, Ö. Hydrogen generation from catalytic hydrolysis of sodium borohydride by a novel Co(II)–Cu(II) based complex catalyst. *J. Power Sour.* **217**, 256–261. https://doi.org/10.1016/j.jpowsour.2012.06.018 (2012).
7. Brack, P., Dann, S. E. & Wijayantha, K. G. U. Heterogeneous and homogenous catalysts for hydrogen generation by hydrolysis of aqueous sodium borohydride ($NaBH_4$) solutions. *Energy Sci. Eng.* **3**, 174–188. https://doi.org/10.1002/ese3.67 (2015).
8. Amendola, S. C. *et al.* An ultrasafe hydrogen generator: Aqueous, alkaline borohydride solutions and Ru catalyst. *J. Power Sour.* **85**, 186–189. https://doi.org/10.1016/s0378-7753(99)00301-8 (2000).
9. Schlesinger, H. I. *et al.* Sodium borohydride, its hydrolysis and its use as a reducing agent and in the generation of hydrogen. *J. Am. Chem. Soc.* **75**, 215–219. https://doi.org/10.1021/ja01097a057 (1953).
10. Lu, Y.-C., Chen, M.-S. & Chen, Y.-W. Hydrogen generation by sodium borohydride hydrolysis on nanosized CoB catalysts supported on TiO_2, Al_2O_3 and CeO_2. *Int. J. Hydrog. Energy* **37**, 4254–4258. https://doi.org/10.1016/j.ijhydene.2011.11.105 (2012).
11. Bozkurt, G., Özer, A. & Yurtcan, A. B. Development of effective catalysts for hydrogen generation from sodium borohydride: Ru, Pt, Pd nanoparticles supported on Co_3O_4. *Energy* **180**, 702–713. https://doi.org/10.1016/j.energy.2019.04.196 (2019).
12. Abdelhamid, H. N. UiO-66 as a catalyst for hydrogen production via the hydrolysis of sodium borohydride. *Dalton Trans.* **49**, 10851–10857. https://doi.org/10.1039/d0dt01688h (2020).
13. Liu, B. H., Li, Z. P. & Suda, S. Solid sodium borohydride as a hydrogen source for fuel cells. *J. Alloy. Compd.* **468**, 493–498. https://doi.org/10.1016/j.jallcom.2008.01.023 (2009).
14. Patel, N. *et al.* Thin films of Co–B prepared by pulsed laser deposition as efficient catalysts in hydrogen producing reactions. *Appl. Catal. A* **323**, 18–24. https://doi.org/10.1016/j.apcata.2007.01.053 (2007).
15. Shu, H. *et al.* Ultra small cobalt nanoparticles supported on MCM41: One-pot synthesis and catalytic hydrogen production from alkaline borohydride. *Catal. Commun.* **118**, 30–34. https://doi.org/10.1016/j.catcom.2018.09.012 (2019).
16. Minkina, V. G., Shabunya, S. I., Kalinin, V. I. & Smirnova, A. Hydrogen generation from sodium borohydride solutions for stationary applications. *Int. J. Hydrog. Energy* **41**, 9227–9233. https://doi.org/10.1016/j.ijhydene.2016.03.063 (2016).
17. Fiorenza, R., Crisafulli, C. & Scirè, S. H_2 purification through preferential oxidation of CO over ceria supported bimetallic Au-based catalysts. *Int. J. Hydrog. Energy* **41**, 19390–19398. https://doi.org/10.1016/j.ijhydene.2016.05.114 (2016).
18. Fiorenza, R., Scirè, S. & Venezia, A. M. Carbon supported bimetallic Ru-Co catalysts for H_2 production through $NaBH_4$ and NH_3BH_3 hydrolysis. *Int. J. Energy Res.* **42**, 1183–1195. https://doi.org/10.1002/er.3918 (2018).
19. Crisafulli, C., Galvagno, S., Maggiore, R., Scire, S. & Saeli, A. Performance of supported Ru-Cu bimetallic catalysts prepared from nitrate precursors. *Catal. Lett.* **6**, 77–83. https://doi.org/10.1007/bf00764055 (1990).
20. Krishnan, P., Yang, T.-H., Lee, W.-Y. & Kim, C.-S. PtRu-$LiCoO_2$ an efficient catalyst for hydrogen generation from sodium borohydride solutions. *J. Power Sour.* **143**, 17–23. https://doi.org/10.1016/j.jpowsour.2004.12.007 (2005).
21. Rachiero, G. P., Demirci, U. B. & Miele, P. Bimetallic RuCo and RuCu catalysts supported on γ-Al_2O_3. A comparative study of their activity in hydrolysis of ammonia-borane. *Int. J. Hydrog. Energy* **36**, 7051–7065. https://doi.org/10.1016/j.ijhydene.2011.03.009 (2011).

22. Dai, H., Qiu, Y.-P., Dai, H.-B. & Wang, P. Ni–Pt/CeO_2 Loaded on granular activated carbon: An efficient monolithic catalyst for controlled hydrogen generation from hydrous hydrazine. *ACS Sustain. Chem. Eng.* **6**, 9876–9882. https://doi.org/10.1021/acssuschemeng.8b01098 (2018).
23. Şahin, Ö., Kilinç, D. & Saka, C. Hydrogen production by catalytic hydrolysis of sodium borohydride with a bimetallic solid-state Co-Fe complex catalyst. *Sep. Sci. Technol.* **50**, 2051–2059. https://doi.org/10.1080/01496395.2015.1016040 (2015).
24. Kılınç, D., Şahin, Ö. & Saka, C. Investigation on salisylaldimine-Ni complex catalyst as an alternative to increasing the performance of catalytic hydrolysis of sodium borohydride. *Int. J. Hydrog. Energy* **42**, 20625–20637. https://doi.org/10.1016/j.ijhydene.2017.06.230 (2017).
25. Kunz, S. *et al.* Size-selected clusters as heterogeneous model catalysts under applied reaction conditions. *Phys. Chem. Chem. Phys.* **12**, 10288. https://doi.org/10.1039/c0cp00288g (2010).
26. Farrag, M. Monodisperse and polydisperse platinum nanoclusters supported over TiO_2 anatase as catalysts for catalytic oxidation of styrene. *J. Mol. Catal. A: Chem.* **413**, 67–76. https://doi.org/10.1016/j.molcata.2015.12.011 (2016).
27. Farrag, M. Enantioselective silver nanoclusters: Preparation, characterization and photoluminescence spectroscopy. *Mater. Chem. Phys.* **180**, 349–356. https://doi.org/10.1016/j.matchemphys.2016.06.017 (2016).
28. Farrag, M., Das, M. K., Moody, M. & Samy El-Shall, M. Ligand-protected ultrasmall Pd nanoclusters supported on metal oxide surfaces for CO oxidation: Does the ligand activate or passivate the Pd nanocatalyst?. *ChemPhysChem* **22**, 312–322. https://doi.org/10.1002/cphc.202000656 (2020).
29. Farrag, M., Thämer, M., Tschurl, M., Bürgi, T. & Heiz, U. Preparation and spectroscopic properties of monolayer-protected silver nanoclusters. *J. Phys. Chem. C* **116**, 8034–8043. https://doi.org/10.1021/jp210453v (2012).
30. Farrag, M., Tschurl, M., Dass, A. & Heiz, U. Infra-red spectroscopy of size selected Au25, Au38 and Au144 ligand protected gold clusters. *Phys. Chem. Chem. Phys.* **15**, 12539. https://doi.org/10.1039/c3cp51406d (2013).
31. Farrag, M., Tschurl, M. & Heiz, U. Chiral gold and silver nanoclusters: Preparation, size selection, and chiroptical properties. *Chem. Mater.* **25**, 862–870. https://doi.org/10.1021/cm3033725 (2013).
32. Farrag, M. Microwave-assisted synthesis of ultra small bare gold clusters supported over Al_2O_3 and TiO_2 as catalysts in reduction of 4-nitrophenol to 4-aminophenol. *Microporous Mesoporous Mater.* **232**, 248–255. https://doi.org/10.1016/j.micromeso.2016.06.032 (2016).
33. Farrag, M. Preparation of mesoporous palladium nanoclusters supported over hematite (α-Fe_2O_3) for selective catalytic hydrogenation of α, β-unsaturated aldehydes. *Microporous Mesoporous Mater.* **257**, 110–117. https://doi.org/10.1016/j.micromeso.2017.08.022 (2018).
34. Good, J. *et al.* On the functional role of the cerium oxide support in the $Au_{38}(SR)_{24}/CeO_2$ catalyst for CO oxidation. *Catal. Today* **280**, 239–245. https://doi.org/10.1016/j.cattod.2016.04.016 (2017).
35. Nie, X., Qian, H., Ge, Q., Xu, H. & Jin, R. CO oxidation catalyzed by oxide-supported $Au_{25}/(SR)_{18}$ nanoclusters and identification of perimeter sites as active centers. *ACS Nano.* **6**, 6014–6022. https://doi.org/10.1021/nn301019f (2012).
36. Nie, X. *et al.* CeO_2-supported $Au_{38}(SR)_{24}$ nanocluster catalysts for CO oxidation: A comparison of ligand-on and -off catalysts. *Nanoscale* **5**, 5912. https://doi.org/10.1039/c3nr00970j (2013).
37. Li, W. *et al.* Mild activation of CeO_2-supported gold nanoclusters and insight into the catalytic behavior in CO oxidation. *Nanoscale* **8**, 2378–2385. https://doi.org/10.1039/c5nr07498c (2016).
38. Farrag, M. & Mohamed, R. A. Ecotoxicity of ~1 nm silver and palladium nanoclusters protected by L-glutathione on the microbial growth under light and dark conditions. *J. Photochem. Photobiol. A* **330**, 117–125. https://doi.org/10.1016/j.jphotochem.2016.07.027 (2016).
39. Creighton, J. A. & Eadon, D. G. Ultraviolet–visible absorption spectra of the colloidal metallic elements. *J. Chem. Soc Faraday Trans.* **87**, 3881–3891. https://doi.org/10.1039/ft9918703881 (1991).
40. Chen, S. & Kimura, K. Synthesis of thiolate-stabilized platinum nanoparticles in protolytic solvents as isolable colloids. *J. Phys. Chem. B* **105**, 5397–5403. https://doi.org/10.1021/jp0037798 (2001).
41. Hostetler, M. J. *et al.* Alkanethiolate gold cluster molecules with core diameters from 1.5 to 5.2 nm: Core and monolayer properties as a function of core size. *Langmuir* **14**, 17–30. https://doi.org/10.1021/la970588w (1998).
42. Burcham, L. J. & Wachs, I. E. The origin of the support effect in supported metal oxide catalysts: In situ infrared and kinetic studies during methanol oxidation. *Catal. Today* **49**, 467–484. https://doi.org/10.1016/s0920-5861(98)00442-8 (1999).
43. Huang, R., Kim, K., Kim, H. J., Jang, M. G. & Han, J. W. Size-controlled Pd nanoparticles loaded on Co_3O_4 nanoparticles by calcination for enhanced CO oxidation. *ACS Appl. Nano Mater.* **3**, 486–495. https://doi.org/10.1021/acsanm.9b02056 (2020).
44. Yang, N., Ni, S., Sun, Y. & Zhu, Y. A facial strategy to synthesize Pd/Co_3O_4 nanosheets with enhanced performance for methane catalytic oxidation. *Mol. Catal.* **452**, 28–35. https://doi.org/10.1016/j.mcat.2018.03.016 (2018).
45. Matin, M. A., Lee, E., Kim, H., Yoon, W.-S. & Kwon, Y.-U. Rational syntheses of core–shell Fe@(PtRu) nanoparticle electrocatalysts for the methanol oxidation reaction with complete suppression of CO-poisoning and highly enhanced activity. *J. Mater. Chem. A* **3**, 17154–17164. https://doi.org/10.1039/c5ta03809j (2015).
46. Buck, R. P. & Lindner, E. Recommendations for nomenclature of ionselective electrodes (IUPAC Recommendations 1994). *Pure Appl. Chem.* **66**, 2527–2536. https://doi.org/10.1351/pac199466122527 (1994).
47. Fouad, O. A., Ali, G. A. M., El-Erian, M. A. I. & Makhlouf, S. A. Humidity sensing properties of cobalt oxide/silica nanocomposites prepared via sol-gel and related routes. *Nano* https://doi.org/10.1142/S1793292012500385 (2012).
48. Abdel Ghafar, H. H., Ali, G. A. M., Fouad, O. A. & Makhlouf, S. A. Enhancement of adsorption efficiency of methylene blue on Co_3O_4/SiO_2 nanocomposite. *Desalin. Water Treat.* **53**, 2980–2989 (2015).
49. Ali, G. A. M., Fouad, O. A. & Makhlouf, S. A. Structural, optical and electrical properties of sol–gel prepared mesoporous Co_3O_4/SiO_2 nanocomposites. *J. Alloy. Compd.* **579**, 606–611. https://doi.org/10.1016/j.jallcom.2013.07.095 (2013).
50. Fouad, O. A., Makhlouf, S. A., Ali, G. A. M. & El-Sayed, A. Y. Cobalt/silica nanocomposite via thermal calcination-reduction of gel precursors. *Mater. Chem. Phys.* **128**, 70–76. https://doi.org/10.1016/j.matchemphys.2011.02.072 (2011).
51. Patterson, A. The Scherrer formula for X-ray particle size determination. *Phys. Rev.* **56**, 978 (1939).
52. Dimitratos, N. *et al.* Pd and Pt catalysts modified by alloying with Au in the selective oxidation of alcohols. *J. Catal.* **244**, 113–121. https://doi.org/10.1016/j.jcat.2006.08.019 (2006).
53. Kojima, Y. *et al.* Hydrogen generation using sodium borohydride solution and metal catalyst coated on metal oxide. *Int. J. Hydrog. Energy* **27**, 1029–1034. https://doi.org/10.1016/s0360-3199(02)00014-9 (2002).
54. Liu, R. S. *et al.* Investigation on mechanism of catalysis by Pt–LiCoO2 for hydrolysis of sodium borohydride using X-ray absorption. *J. Phys. Chem. B* **112**, 4870–4875. https://doi.org/10.1021/jp075592n (2008).
55. Hung, T.-F. *et al.* An alternative cobalt oxide-supported platinum catalyst for efficient hydrolysis of sodium borohydride. *J. Mater. Chem.* **21**, 11754–11759. https://doi.org/10.1039/C1JM11720C (2011).
56. Andrieux, J., Demirci, U. B. & Miele, P. Langmuir-Hinshelwood kinetic model to capture the cobalt nanoparticles-catalyzed hydrolysis of sodium borohydride over a wide temperature range. *Catal. Today* **170**, 13–19. https://doi.org/10.1016/j.cattod.2011.01.019 (2011).
57. Su, C.-C., Lu, M.-C., Wang, S.-L. & Huang, Y.-H. Ruthenium immobilized on Al_2O_3 pellets as a catalyst for hydrogen generation from hydrolysis and methanolysis of sodium borohydride. *RSC Adv.* **2**, 2073–2079 (2012).
58. Peña-Alonso, R., Sicurelli, A., Callone, E., Carturan, G. & Raj, R. A picoscale catalyst for hydrogen generation from $NaBH_4$ for fuel cells. *J. Power Sour.* **165**, 315–323. https://doi.org/10.1016/j.jpowsour.2006.12.043 (2007).

59. Peng, S., Fan, X., Zhang, J. & Wang, F. A highly efficient heterogeneous catalyst of Ru/MMT: Preparation, characterization, and evaluation of catalytic effect. *Appl. Catal. B* **140–141**, 115–124. https://doi.org/10.1016/j.apcatb.2013.03.029 (2013).
60. Liang, Y., Dai, H.-B., Ma, L.-P., Wang, P. & Cheng, H.-M. Hydrogen generation from sodium borohydride solution using a ruthenium supported on graphite catalyst. *Int. J. Hydrogen Energy* **35**, 3023–3028. https://doi.org/10.1016/j.ijhydene.2009.07.008 (2010).

Acknowledgements
This work was financially supported by Assiut University, Egypt.

Author contributions
M.F. wrote the main manuscript text and prepared Figs. 1, 2, 3, 4, 5, 6, 7, 8, 9 and 10. All authors reviewed the manuscript.

Funding
Open access funding provided by The Science, Technology & Innovation Funding Authority (STDF) in cooperation with The Egyptian Knowledge Bank (EKB).

Competing interests
The authors declare no competing interests.

Additional information
Supplementary Information The online version contains supplementary material available at https://doi.org/10.1038/s41598-022-21064-z.

Correspondence and requests for materials should be addressed to M.F.

Reprints and permissions information is available at www.nature.com/reprints.

Publisher's note Springer Nature remains neutral with regard to jurisdictional claims in published maps and institutional affiliations.